# SENSITIVITY AND UNCERTAINTY ANALYSIS OF AERODYNAMIC FLOWS

**Dominique Pelletier , Éric Turgeon , Jeff Borggaard**
**Canada Research Chair**
**École Polytechnique de Montréal**
**P.O. Box 6079, Station Centre-ville**
**Montréal, Canada, H3C 3A7**
**e-mail: Dominique.Pelletier@polymtl.ca**

**Keywords:** *Sensitivity analysis, Uncertainty analysis, Aerodynamic flows*

## Abstract

*This paper presents a methodology for cascading uncertainties in input parameters through a CFD model to obtain uncertainty estimates of output flow variables or output functionals such as lift, drag and moment coefficients for airfoils. The sensitivity equation method is used to derive flow sensitivity equations which are then solved by an adaptive finite element method. Sensitivity information is then used to perform uncertainty analysis for turbulent flows over a backward facing step and over a NACA 0012 airfoil.*

## 1 Introduction

In all practical CFD applications, parameters governing the flow are known only to a certain level of accuracy or uncertainty. Such parameters may appear in boundary conditions, fluid properties, closure coefficients, geometry, etc. In many situations the effects of such data uncertainties on the flow response is negligible. In other cases it is not. From a design standpoint, assessing the response of the flow to these uncertainties is of prime importance. We use sensitivity information to propagate uncertainty in the input data into uncertainty in the flow solution. Initial work by Blackwell *et al.* [2] was limited to the heat equation with constant physical properties. Putko *et al.* [8] used automatic differentiation to perform uncertainty analysis of quasi-one-dimensional Euler equations. Recent work by the authors discusses sensitivity for laminar flows with variable properties and for $k-\varepsilon$ modeling of turbulent flows [10, 11, 12, 13].

The paper is organized as follows. The flow equations and boundary conditions are presented first. Next, the sensitivities and their use for uncertainty analysis are described. The methodology is then applied to flow over a backward facing step and around a NACA 0012 airfoil. Uncertainty estimates are obtained for flow variables, skin friction, and aerodynamic coefficients. As a by-product, the airfoil stability derivatives are obtained at little additional cost.

## Flow Equations

The flow regime of interest is modeled by the time-averaged momentum and continuity equations,

$$\rho\mathbf{u}\cdot\nabla\mathbf{u} = -\nabla p + \nabla\cdot\left[(\mu+\mu_t)\left(\nabla\mathbf{u}+\nabla\mathbf{u}^T\right)\right] \quad (1)$$

$$\nabla\cdot\mathbf{u} = 0, \quad (2)$$

where $\rho$ is the density, $\mathbf{u}$ is the velocity, $p$ is the pressure, and $\mu$ is the viscosity. The eddy viscosity $\mu_t$ is computed using the $k-\varepsilon$ turbulence

model [7]:

$$\mu_t = \rho C_\mu \frac{k^2}{\varepsilon}.$$

The logarithmic form of the turbulence equations is used to preserve positivity [5]. This is equivalent to the following change of variables:

$$\mathcal{K} = \ln(k) \quad \text{and} \quad \mathcal{E} = \ln(\varepsilon).$$

The transport equations for $\mathcal{K}$ and $\mathcal{E}$ are:

$$\rho \mathbf{u} \cdot \nabla \mathcal{K} = \nabla \cdot \left[ \left( \mu + \frac{\mu_t}{\sigma_k} \right) \nabla \mathcal{K} \right] \tag{3}$$
$$+ \left( \mu + \frac{\mu_t}{\sigma_k} \right) \nabla \mathcal{K} \cdot \nabla \mathcal{K} + \mu_t e^{-\mathcal{K}} P - \rho^2 C_\mu \frac{e^{\mathcal{K}}}{\mu_t}$$

$$\rho \mathbf{u} \cdot \nabla \mathcal{E} = \nabla \cdot \left[ \left( \mu + \frac{\mu_t}{\sigma_\varepsilon} \right) \nabla \mathcal{E} \right] \tag{4}$$
$$+ \left( \mu + \frac{\mu_t}{\sigma_\varepsilon} \right) \nabla \mathcal{E} \cdot \nabla \mathcal{E} + \rho C_1 C_\mu e^{\mathcal{K}-\mathcal{E}} P$$
$$- C_2 \rho e^{\mathcal{E}-\mathcal{K}}$$

The constants $C_1$, $C_2$, $C_\mu$, $\sigma_k$, and $\sigma_\varepsilon$ are set to the values recommended by Launder and Spalding [7] and given in Table 1.

| $C_\mu$ | $C_1$ | $C_2$ | $\sigma_k$ | $\sigma_\varepsilon$ |
|---|---|---|---|---|
| 0.09 | 1.44 | 1.92 | 1.0 | 1.3 |

**Table 1** Constants for the $k-\varepsilon$ model

A two-velocity scales wall function provides boundary conditions near solid walls [11]:

$$u^+ = \begin{cases} y^+ & \text{for } y^+ < y_c^+ \\ \frac{1}{\kappa} \ln(E y^+) & \text{for } y^+ \geq y_c^+ \end{cases}, \tag{5}$$

where $\kappa$ is the Kármán constant and $E$ a roughness parameter. The dimensionless distance to the wall $y^+$ and the dimensionless tangential velocity $u^+$ are given by:

$$y^+ = \frac{\rho y u_k}{\mu} \qquad u^+ = \frac{u_t}{u_{**}} \tag{6}$$

These wall functions involve two velocity scales: $u_{**}$, the friction velocity, and $u_k$, a velocity scale based on the turbulent kinetic energy defined as

$$u_k = C_\mu^{1/4} k^{1/2}, \tag{7}$$

where $k$ is taken at the boundary of the computational domain. The boundary conditions for $k$, $\varepsilon$, and the momentum equations at a distance $y = d$ to the wall are:

$$\frac{\partial k}{\partial n} = 0 \qquad \varepsilon = \frac{u_k^3}{\kappa d}$$
$$\mathbf{u} \cdot \hat{\mathbf{n}} = 0 \qquad \tau_w = \rho u_{**} u_k.$$

## Sensitivity Equations

The continuous sensitivity equations (CSE) are derived by implicit differentiation of the flow equations (1) and (2) with respect to parameter $a$. Thus, not only do we treat the variable $\mathbf{u}$ as a function of space, but also as a function of the parameter $a$. This dependence is denoted as $\mathbf{u}(\mathbf{x}; a)$. We define the flow sensitivities as the partial derivatives $\mathbf{s}_u = \frac{\partial \mathbf{u}}{\partial a}$ and $s_p = \frac{\partial p}{\partial a}$. The derivatives of the fluid properties and other flow parameters are denoted using a ($'$). The general approach used to derive the CSE is described in detail by Turgeon *et al.* [12]. For example, if the parameter of interest is the closure coefficient $C_2$, then the sensitivity equations are:

$$\rho \mathbf{s}_u \cdot \nabla \mathbf{u} + \rho \mathbf{u} \cdot \nabla \mathbf{s}_u = -\nabla s_p$$
$$+ \nabla \cdot \left[ \mu_t' \left( \nabla \mathbf{u} + (\nabla \mathbf{u})^T \right) \right.$$
$$\left. + (\mu + \mu_t) \left( \nabla \mathbf{s}_u + (\nabla \mathbf{s}_u)^T \right) \right]$$
$$\nabla \cdot \mathbf{s}_u = 0.$$

A similar approach is applied to obtain the sensitivity equations of the turbulence variables. Implicit differentiation of the flow boundary conditions (Dirichlet, Neumann and wall functions) yields the required boundary conditions for the sensitivities [12].

## Finite Element Solver

The flow and sensitivity equations are solved by the same adaptive finite element method. Ele-

ment matrices are constructed using a numerical Jacobian technique. When needed, stabilization terms are added to the standard Galerkin formulation. The accuracy of the solution is controlled by an adaptive remeshing strategy. In our approach errors in all variables (including sensitivities) are analyzed and contribute to the mesh adaptation process. Error estimates are obtained by a local least-squares reconstruction of the solution derivatives [14]. The adaptive methodology is used to generate grid converged solutions.

## Uncertainty Analysis

We consider here that the flow solution depends on some parameters $\mathbf{a} = (a_1, a_2, ..., a_n)$ describing geometry, boundary conditions, fluid properties, or flow model. If $\mathbf{a}$ has a small uncertainty $\Delta\mathbf{a}$, a first order Taylor series yields the following approximation of the velocity uncertainty $\Delta u$:

$$|\Delta u| \approx \sum_{i=1}^{n} \left| \frac{\partial u}{\partial a_i}(x, y; \mathbf{a}) \right| |\Delta a_i| \,. \qquad (8)$$

The uncertainty $\Delta u$ on the flow response can be viewed as a worst case scenario in which the uncertainty contribution due to input uncertainties $\Delta a_i$ all add up in absolute value. Other formulas for the uncertainty yield more optimistic uncertainty estimates [8].

## Numerical Results

### Backward Facing Step

We first demonstrate our approach to uncertainty analysis by applying it to turbulent flow over a backward facing step as studied experimentally by Kim [6]. The Reynolds number is $\mathrm{Re} = 47,625$. The complete statement of the computational model is found elsewhere [11].

The uncertainty bound (8) is used to propagate the uncertainties in the parameters $C_\mu$, $C_1$, $C_2$, $\sigma_k$, and $\sigma_\varepsilon$ into the CFD solution. As a first approximation, we consider that these coefficients are accurate to within one half unit of the rightmost digit. Table 2 summarizes the uncertainties in the coefficients used in the present study. Note that the "accuracy" of the coefficients is probably lower than this.

| $\Delta C_\mu$ | $\Delta C_1$ | $\Delta C_2$ | $\Delta\sigma_k$ | $\Delta\sigma_\varepsilon$ |
|---|---|---|---|---|
| 0.005 | 0.005 | 0.005 | 0.05 | 0.05 |

**Table 2** Uncertainties of the closure coefficients

Figure 1 presents the prediction of the horizontal component of velocity at $x/L = 8$. The selected uncertainties in the coefficient values do not explain the differences observed between numerical results and experimental measurements. In fact, the predicted uncertainties on $u$ are quite small.

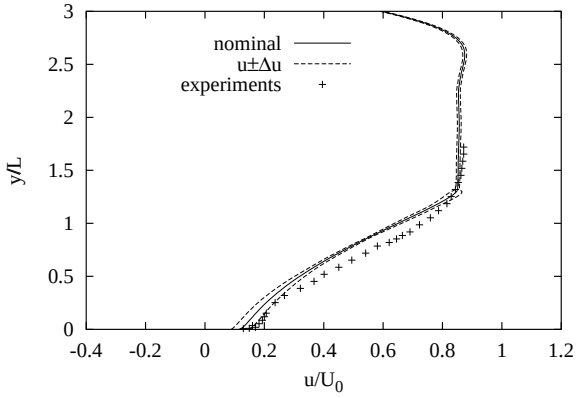


**Fig. 1** Step: uncertainty in $u$ at $x/L = 8$

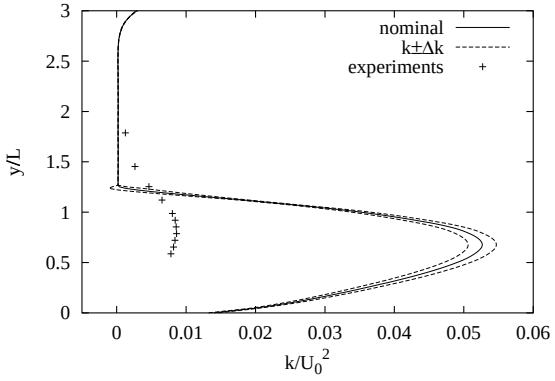


**Fig. 2** Step: uncertainty in $k$ at $x/L = 5.8$

Figure 2 compares the numerical predictions of $k$, the turbulent kinetic energy (TKE), with its

uncertainty bands, to the experimental measurements of Kim [6]. Clearly, the predictions are poor, even if we consider the uncertainties.

We now turn our attention to the assessment of uncertainty in the predictions of the skin friction coefficient, a derived quantity, defined as:

$$C_f = \frac{\tau_w}{\frac{1}{2}\rho_0 U_0^2}$$

where $U_0$ is a reference velocity. The skin friction sensitivity is given by:

$$C_f' = \frac{\tau_w'}{\frac{1}{2}\rho_0 U_0^2}$$

Recall that $C_f$ depends on the five closure coefficients. Which of these parameters exerts the strongest influence on $C_f$ is difficult to determine by direct comparisons of the sensitivities. A solution to this problem is to scale the sensitivity values by the nominal (reference) values of the parameter [2]. The resulting *scaled sensitivities* have the form

$$\frac{\partial \mathbf{u}}{\partial a} a_0, \quad \frac{\partial p}{\partial a} a_0 \quad \text{etc.},$$

where $a_0$ is the nominal value of parameter $a$. In this way, comparing $\frac{\partial C_f}{\partial a} a_0$ with $\frac{\partial C_f}{\partial b} b_0$ is more meaningful since they both have the same units even if $a$ and $b$ do not.

The scaled sensitivities of $C_f$ along the bottom wall are plotted in Figure 3. It shows that $C_f$ is most sensitive to $C_1$ and $C_2$. The sensitivities are maximum for $x/L$ around 6 or 7, which corresponds to the reattachment point. On the other hand, sensitivities are very small around $x/L = 4$ where $C_f$ exhibits a minimum (see Figure 4). The prediction of $C_f$ and its uncertainty band are plotted in Figure 4. The uncertainties are larger where the scaled sensitivities of $C_f$ are larger. Figure 5 compares the contribution of each parameter to the total uncertainty on $C_f$. As can be seen, the largest contribution is from $C_\mu$ (because of its large uncertainty) whereas the smallest is from $\sigma_\varepsilon$. All parameters contribute significantly to the uncertainty on $C_f$. The discussion would not be complete without a grid

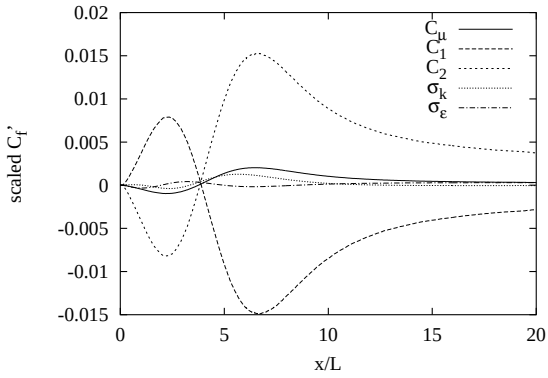


**Fig. 3** Step: scaled $C_f'$

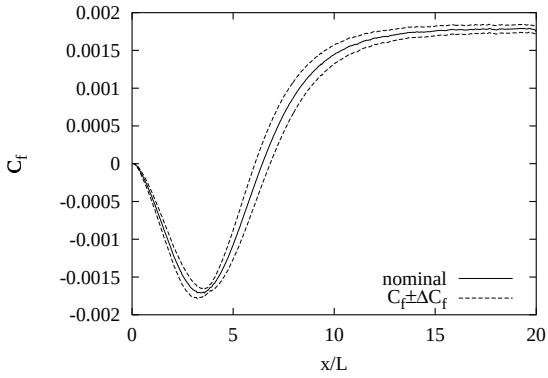


**Fig. 4** Step: uncertainty on $C_f$

convergence study. Figures 6 and 7 present the grid convergence of $C_f$ and a typical scaled sensitivity, $C_1 \frac{\partial C_f}{\partial C_1}$. These quantities are almost grid converged, with only small differences between the two finest meshes. When performing uncertainty analysis with very small data uncertainties, it is necessary and important to reduce numerical errors to negligible levels to ensure a rigorous uncertainty assessment. This is not completely achieved here even with our mesh adaptation strategy. However, the numerical errors are smaller than the predicted uncertainties. We end the discussion of this example by looking at the uncertainty on the location $x_r$ of the reattachment point which is defined as the point where $u = 0$ on the lower computational boundary modeled with a wall function. The material derivative of $u$ following the re-attachment point when $a$ changes

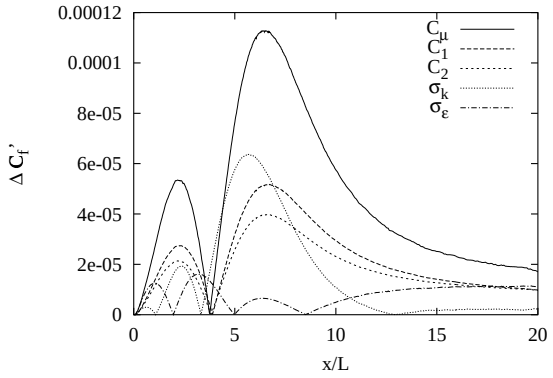


**Fig. 5** Step: contributions to the uncertainty on $C_f$

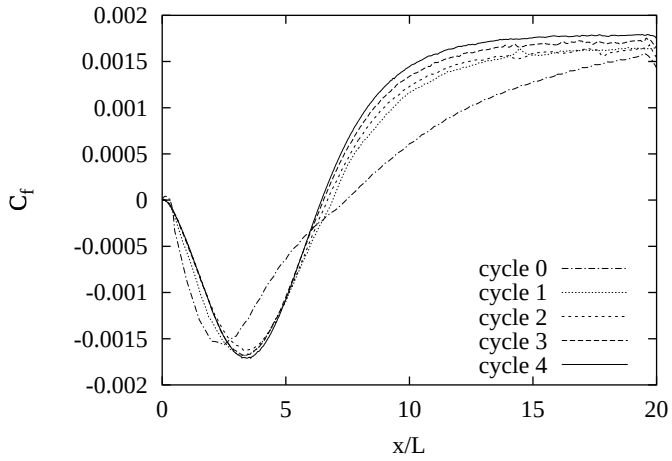


**Fig. 6** Backward facing step: grid convergence of $C_f$

sign must be zero:

$$\frac{Du}{Da} = 0$$

which implies

$$\frac{\partial u}{\partial a} + \frac{\partial u}{\partial x}\frac{\partial x_r}{\partial a} = 0$$

yielding the following expression for the sensitivity $x_r'$:

$$x_r' = -\frac{s_u}{\frac{\partial u}{\partial x}}.$$

The prediction of $x_r$ is about $6.3L$ ($L$ being the step height), with a numerical error of about $0.1L$, whereas the experimental value is $x_r/L = 7 \pm 0.5$ [6]. Numerical results at $x = 6.3L$ are summarized in Table 3. Scaled sensitivities $s_u$ and $x_r'$ indicate that parameters $C_1$ and $C_2$ exert the strongest influence on $x_r$. A 1% change in these parameters result in a $0.2L$ change in $x_r$. Notice, that all parameters except $\sigma_\varepsilon$ contribute significantly to the uncertainty $\Delta x_r$. Contributions of $C_\mu$ and $\sigma_k$ are due to their larger uncertainty. The total uncertainty on $x_r/L$ is 0.37, which means that the predicted uncertainty band overlaps the uncertainty band of the experimental measurements.

| | $C_\mu$ | $C_1$ | $C_2$ | $\sigma_k$ | $\sigma_\varepsilon$ |
|---|---|---|---|---|---|
| $s_u$ | 2.74 | -1.25 | 0.97 | 0.144 | -0.015 |
| scaled $s_u$ | 0.245 | -1.80 | 1.86 | 0.144 | -0.020 |
| $x_r'$ | -31.1 | 14.2 | -11.0 | -1.64 | -0.173 |
| scaled $x_r'$ | -2.80 | 20.4 | -21.1 | -1.64 | -0.225 |
| $\Delta x_r$ | 0.156 | 0.071 | 0.055 | 0.082 | 0.009 |

**Table 3** Backward facing step: uncertainty on $x_r$

## NACA 0012 airfoil

The CSE is now used to produce uncertainty estimates of lift, drag and moment coefficients of a NACA 0012 airfoil due to uncertainties in its angle of attack. An earlier study of sensitivities of airfoils was made by Godfrey *et al.* [3] for laminar flow. It is well known that the standard $k-\varepsilon$ model with wall functions suffers from deficiencies for predicting such turbulent flows. Hence, the present results should be viewed as a demonstration of the CSE and its application to uncertainty analysis. Sensitivity equations can be derived for other turbulence models better suited to airfoil aerodynamics [4].

Computer memory considerations have forced us to use a computational domain of smaller size that is customary in airfoil aerodynamics. The computational domain is a rectangular box extending 10 chords upstream and 3 chords downstream of the airfoil; and 8 chords above and below the airfoil. This choice will induce an error in the airfoil force

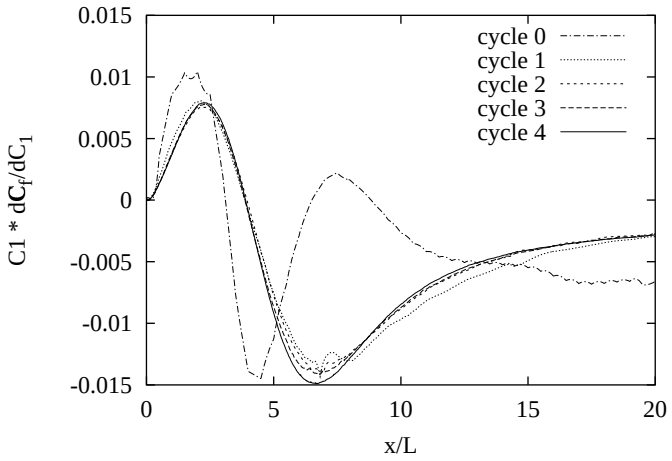


**Fig. 7** Backward facing step: grid convergence of $C_1 \frac{\partial C_f}{\partial C_1}$

coefficients, especially on drag. It is a well documented fact that the location of the outer boundary of the domain induces an error in drag that is ordered in $\frac{1}{L_b}$, where $L_b$ is the distance from the airfoil to the outer boundary. See Roache [9] and Zingg [15] for further discussion.

We reiterate that in light of the above observations, results presented in this section should be viewed as an illustration of the proposed approach to uncertainty analysis. They do not constitute quantitative predictions.

The angle of attack is studied as a value parameter in the inflow boundary conditions given by:

$$u = U_0 \cos(\alpha) \tag{9}$$
$$v = U_0 \sin(\alpha). \tag{10}$$

Wall functions provide boundary conditions on the airfoil boundary and are used to extract surface forces using the following relationships:

$$\begin{aligned}
u_k &= C_\mu^{\frac{1}{4}} \sqrt{k} \\
y^+ &= \frac{u_k d}{\nu} \\
u^+ &= \frac{1}{\kappa} \log E y^+ \\
\vec{u}_{**} &= \frac{1}{u^+} \begin{Bmatrix} U_{tx} \\ V_{ty} \end{Bmatrix} \\
\vec{\tau}_w &= \rho u_k \vec{u}_{**} \\
\begin{Bmatrix} \tau_{wx} \\ \tau_{wy} \end{Bmatrix} &= \rho \kappa C_\mu^{\frac{1}{4}} \frac{\sqrt{k}}{\log \frac{E C_\mu^{\frac{1}{4}} d}{\nu} \sqrt{k}} \begin{Bmatrix} U_{tx} \\ V_{ty} \end{Bmatrix}
\end{aligned}$$

$$\begin{aligned}
\vec{F} &= \oint_C (\vec{\tau_w} + p\vec{n}) dl \\
\begin{Bmatrix} F_x \\ F_y \end{Bmatrix} &= \oint_C \begin{Bmatrix} \tau_w t_x + p n_x \\ \tau_w t_y + p n_y \end{Bmatrix} dl
\end{aligned}$$

$$\begin{aligned}
L &= F_y \cos(\alpha) - F_x \sin(\alpha) \\
D &= F_x \cos(\alpha) + F_y \sin(\alpha) \\
\vec{M} &= \oint_C \vec{OM} \times (\vec{\tau_w} + p\vec{n}) dl \\
M &= \oint_C \left( x - \frac{1}{4} \right) (\tau_w t_y + p n_x) dl \\
&\quad - y(\tau_w t_x + p n_y) dl.
\end{aligned}$$

In these expressions, $\tau_w$ is the wall shear stress, that is the tangential force acting along the surface for the airfoil; $t_x$ and $t_y$ are the components of the unit vector tangent to the airfoil; $n_x$ and $n_y$ are the components of the unit vector normal to the airfoil ; $\vec{F}$ is the total force vector acting on the airfoil, $D$ is the drag, $L$ the lift and $M$ the moment with respect to the quarter chord point. The lift, drag and pitching moment coefficients are obtained as follows:

$$C_L = \frac{L}{\frac{1}{2}\rho_0 U_0^2 A} \tag{11}$$
$$C_D = \frac{D}{\frac{1}{2}\rho_0 U_0^2 A} \tag{12}$$
$$C_M = \frac{M}{\frac{1}{2}\rho_0 U_0^2 A c} \tag{13}$$

where $\rho_0$ and $U_0$ are the free stream density and velocity respectively; $A$ is the wing area and $c$ the chord of the airfoil.

Sensitivity equations are written for computing sensitivities of the flow with respect to the angle of attack. Inflow boundary conditions for the sensitivities are obtained by differentiating equations (9) and (10) with respect to $\alpha$:

$$S_u = -U_0 \sin(\alpha) \quad (14)$$

$$S_v = U_0 \cos(\alpha). \quad (15)$$

Sensitivities of surface forces are obtained by differentiating the wall function relations given above with respect to the angle of attack. This yields:

$$\vec{S}_p = S_p \vec{n}$$

$$\vec{S}_{\tau_w} = \rho \frac{u_k}{u^+} \left\{ \left( 1 - \frac{1}{\kappa u^+} \right) \frac{S_k}{2} \begin{Bmatrix} U_{tx} \\ V_{ty} \end{Bmatrix} + \begin{Bmatrix} S_{U_{tx}} \\ S_{V_{ty}} \end{Bmatrix} \right\}$$

$$\vec{S_{\vec{F}}} = \oint_C (\vec{S}_{\tau_w} + \vec{S}_p) dl$$

$$S_L = \frac{dL}{d\alpha} = S_{F_y} \cos(\alpha) - S_{F_x} \sin(\alpha) - F_y \sin(\alpha) - F_x \cos(\alpha) \quad (16)$$

$$S_D = \frac{dD}{d\alpha} = S_{F_x} \cos(\alpha) + S_{F_y} \sin(\alpha) - F_x \sin(\alpha) + F_y \cos(\alpha) \quad (17)$$

$$S_{\vec{M}} = \frac{d\vec{M}}{d\alpha} = \oint_C (\vec{OM} \times (\vec{S_{\tau_w}} + \vec{S_p}))\vec{k} dl$$

$$S_M = \frac{dM}{d\alpha} = \oint_C \left( x - \frac{1}{4} \right) (S_{\tau_w} t_y + S_p n_x) dl - y (S_{\tau_w} t_x + S_p n_y) dl. \quad (18)$$

The stability derivatives are the sensitivities of the aerodynamic coefficients. They are obtained by differentiating equations (11) to (13) with respect to $\alpha$ and by noting that the denominators are independent of $\alpha$

$$\frac{dC_L}{d\alpha} = \frac{S_L}{\frac{1}{2}\rho_0 U_0^2 A} \quad (19)$$

$$\frac{dC_D}{d\alpha} = \frac{S_D}{\frac{1}{2}\rho_0 U_0^2 A} \quad (20)$$

$$\frac{dC_M}{d\alpha} = \frac{S_M}{\frac{1}{2}\rho_0 U_0^2 A c} \quad (21)$$

where $S_L$, $S_D$ and $S_M$ are evaluated from equations (16)-(18)

In the results presented below, adaptation is driven by error estimates on the velocity, turbulence variables and eddy viscosity. The pressure is not included in the mesh adaptation process. This approach leads to more clustering of grid points near the airfoil than when pressure is included. Auxiliary computations including adaptation with respect to pressure revealed that neglecting pressure in the adaptation process has no measurable negative impact on the solution accuracy. Figure 8 shows the mesh after 5 cycles of adaptation. Figure 9 shows the trajectory of the global errors for all solution fields. It confirms that our mesh adaptation strategy leads to solution improvements for all dependent variables.

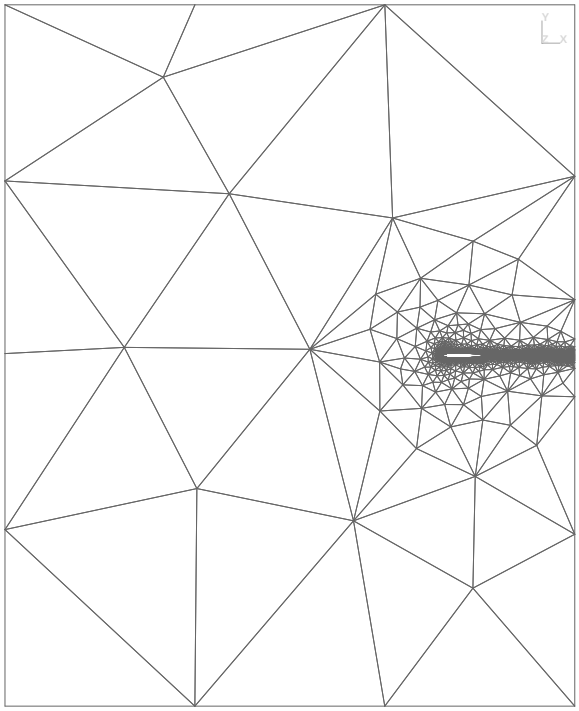

**Fig. 8** Final mesh, adaptation without pressure

Typical grid convergence of the surface pressure distribution is shown in Figures 10 and 11. As can be seen the surface pressure is grid converged.

Similar results for the lift, drag and moment coefficients and their sensitivities, were observed at all angles of attack. Figures 12 and 13 present

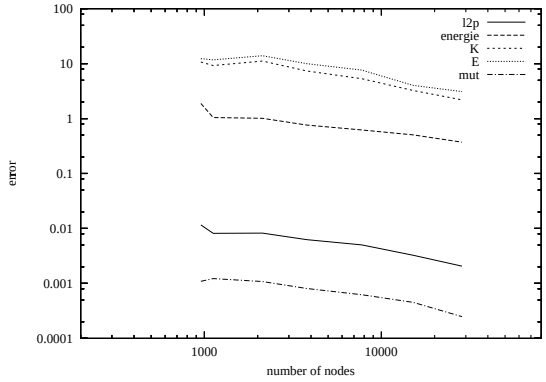


**Fig. 9** Error trajectories, adaptation without pressure

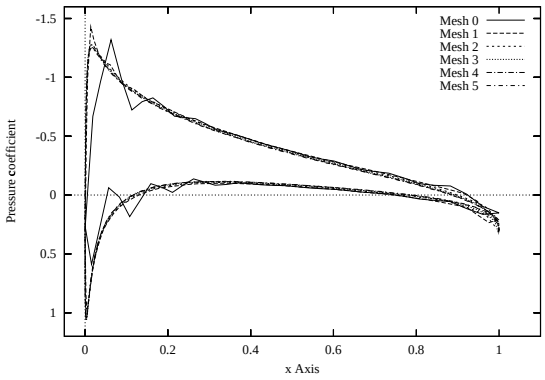


**Fig. 10** NACA0012: Grid convergence of surface pressure at $\alpha = 4$ degrees

grid convergence of the aerodynamic coefficients and their sensitivities. Note that grid convergence is different for each sensitivity [9].

Prediction of $C_L$, $C_D$ and $C_M$ are shown in Figures 14, 15 and 16 along with their sensitivities $\frac{dC_L}{d\alpha}$, $\frac{dC_D}{d\alpha}$, $\frac{dC_M}{d\alpha}$. The predictions for lift and moment coefficients are in agreement with the data found in Abbott *et al.* [1]. The levels of predicted drag do not agree with those reported by Abbott *et al.*. This might be due to the reduced extent of our computational domain. However, trends of $C_D$ agree with those of the measurements [1]. The predicted sensitivity derivatives $\frac{dC_L}{d\alpha}$, $\frac{dC_D}{d\alpha}$, $\frac{dC_M}{d\alpha}$ are in good agreement with the observed slopes of the lift, drag, and moment coefficients of Figures 14, 15 and 16.

Finally, the uncertainty in the angle of attack is propagated through the CFD into uncertainty bands for lift, drag and moment coefficients. For illustration purposes and for simplicity we use $\Delta\alpha_0 = 1$ degree at all angles of attacks. See Figures 14 to 16. Variations in the width of the uncertainty bands are caused by changes in the magnitude of the sensitivities. In particular, the drag coefficient has a zero sensitivity at zero degrees. Hence, the uncertainty also vanishes at this angle.

## Conclusions

The CSE is used to perform uncertainty analysis on the standard $k-\varepsilon$ model of turbulence. The method can predict uncertainty estimates of flow variables (velocity, pressure, turbulent kinetic energy), of derived quantities (skin friction) or of integral quantities (lift, drag and moment coefficient). The methodology was applied to turbulent flow over a backward facing step to assess the effect of uncertainties of the closure coefficients on flow predictions: velocity, TKE and skin friction. The methodology was also applied to predict uncertainty bands on the lift, drag and moment coefficients of NACA 0012 airfoils for angles of attack ranging from 0 to 10 degrees.

## Acknowledgments

This work was sponsored in part by NSERC (Government of Canada), FCAR (Government

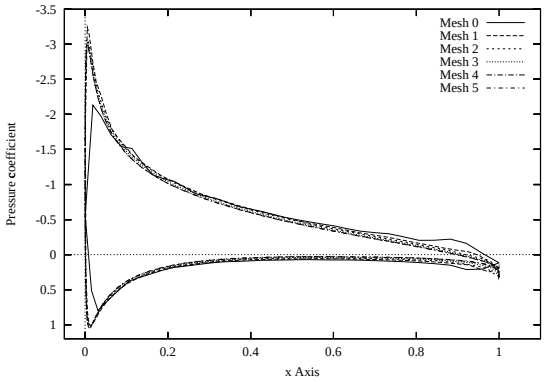


**Fig. 11** NACA0012: Grid convergence of surface pressure at $\alpha = 8$ degrees

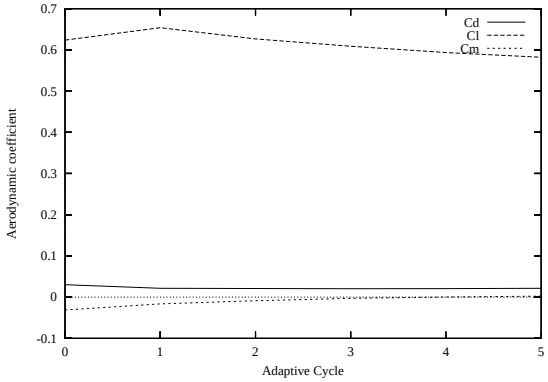


**Fig. 12** Grid convergence of aerodynamics coefficients at 6 degrees

of Québec), the Canada Research Chair Program and by the Air Force Office of Scientific Research under grant AFOSR F49620-00-1-0299.

## References

[1] Abbott I and Von Doenhoff A. *Theory of Wing Sections.* Dover Publications, New York, 1959.

[2] Blackwell B. F, Dowding K. J, Cochran R. J, and Dobranich D. Utilization of sensitivity coefficients to guide the design of a thermal battery. *Proc ASME IMECE*, Vol. 361, pp 73–82, Anaheim, CA, Nov. 1998.

[3] Godfrey A. G and Cliff E. M. Direct calculation of aerodynamic force derivatives: A sensitivity-equation approach. *Proc 36th AIAA Aerospace Sciences Meeting and Exhibit*, Reno, NV, Jan. 1998. AIAA Paper 98-0393.

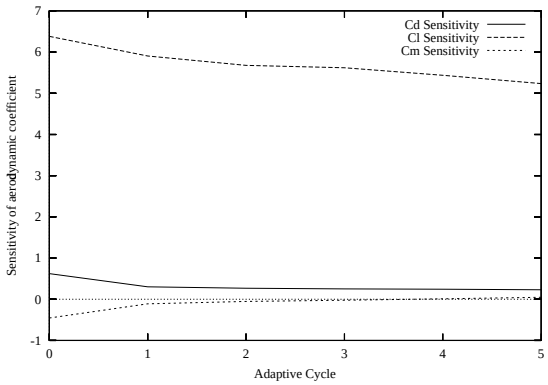


**Fig. 13** Grid convergence of aerodynamics coefficients sensitivities at 6 degrees

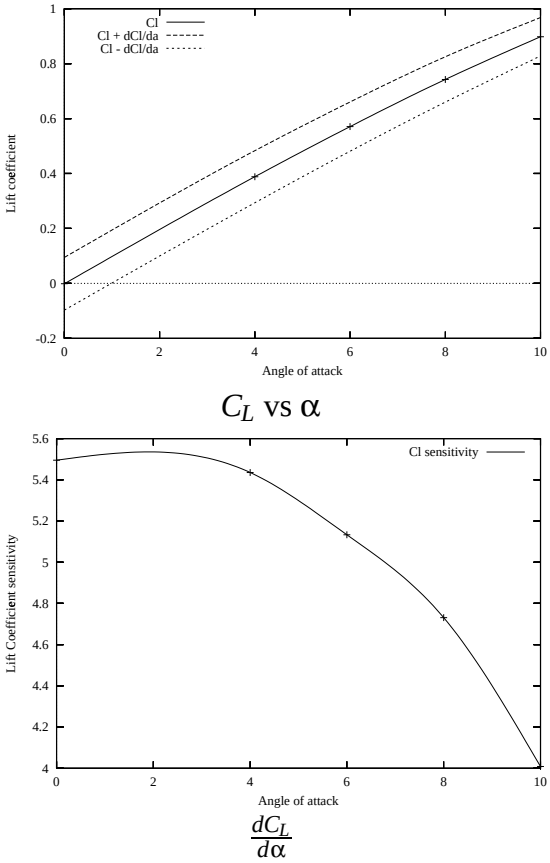


**Fig. 14** Lift coefficient and it sensitivity with respect to α

[4] Godfrey A. G and Cliff E. M. Sensitivity equations for turbulent flows. *Proc 39th AIAA Aerospace Sciences Meeting and Exhibit*, Reno, NV, Jan. 2001. AIAA Paper 2001-1060.

[5] Ilinca F and Pelletier D. Positivity preservation and adaptive solution for the $k-\varepsilon$ model of turbulence. *AIAA Journal*, Vol. 36, No 1, pp 44–51, 1998.

[6] Kim J. J. *Investigation of separation and reattachment of turbulent shear layer: Flow over a backward facing step.* PhD thesis, Stanford University, 1978.

[7] Launder B. E and Spalding J. The numerical computation of turbulent flows. *Computer Methods in Applied Mechanics and Engineering*, pp 269–289, 1974.

[8] Putko M, Newman P, Taylor III A, and Green L. Approach for uncertainty propagation and ro-

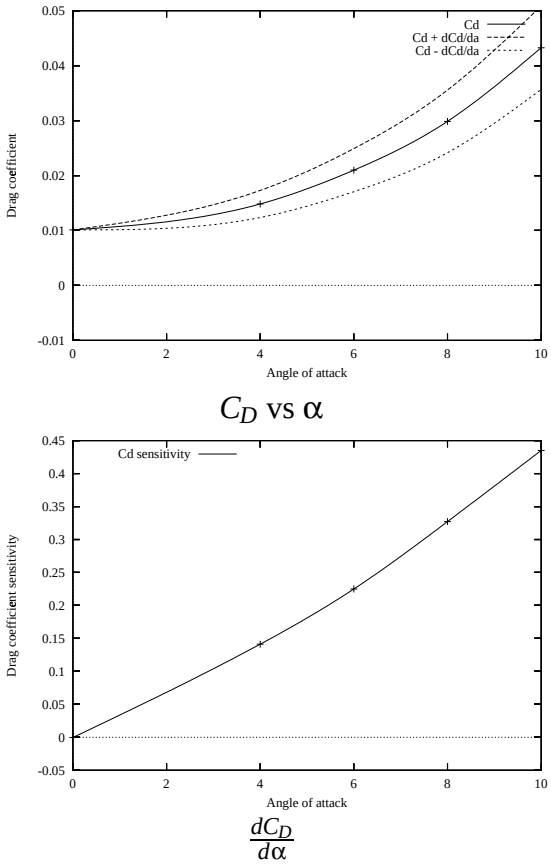


**Fig. 15** Drag coefficient and its sensitivity with respect to α

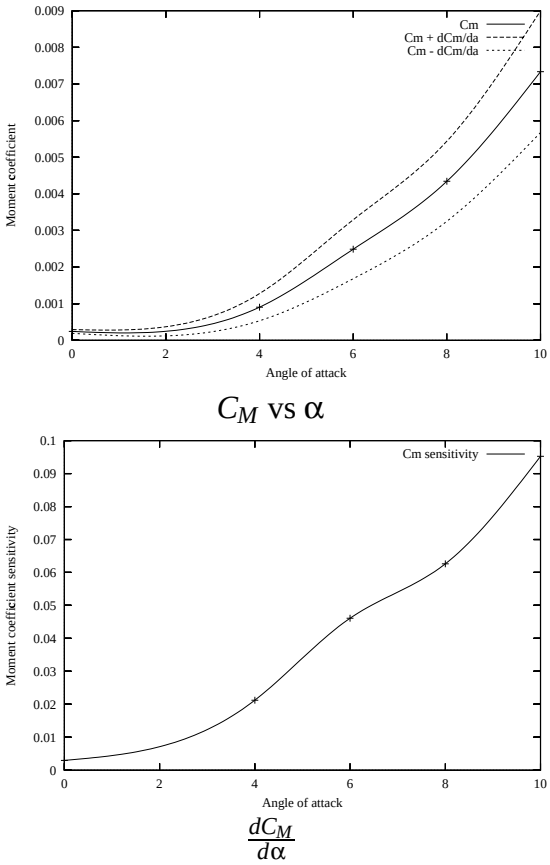


**Fig. 16** Moment coefficient and its sensitivity with respect to α

bust design in cfd using sensitivity derivatives. *Proc 15th AIAA Computational Fluid Dynamics Conference*, Anaheim, CA, Jun. 2001. AIAA Paper 2001-2528.

[9] Roache P. *Verification and Validation in Computational Science and Engineering.* Hermosa publishers, Albuquerque, NM, 1998.

[10] Turgeon , Pelletier D, Étienne S, and Borggaard J. Sensitivity and uncertainty analysis for turbulent flows. *Proc 40th AIAA aerospace Sciences Meeting and Exhibit*, Reno, NV, Jan. 2002. AIAA Paper 2002-0985.

[11] Turgeon É, Pelletier D, and Borggaard J. Application of a sensitivity equation method to the the $k-\varepsilon$ model of turbulence. *Proc 15th AIAA Computational Fluid Dynamics Conference*, Anaheim, CA, Jun. 2001. AIAA Paper 2001-2534.

[12] Turgeon É, Pelletier D, and Borggaard J. A general continuous sensitivity equation formulation for the $k-\varepsilon$ model of turbulence. *Proc 31st AIAA Fluid Dynamics Conference and EXhibit*, Anaheim, CA, Jun. 2001. AIAA Paper 2001-3000.

[13] Turgeon É, Pelletier D, and Borggaard J. Sensitivity and uncertainty analysis for variable property flows. *Proc 39th AIAA Aerospace Sciences Meeting and Exhibit*, Reno, NV, Jan. 2001. AIAA Paper 2001-0139.

[14] Zienkiewicz O. C and Zhu J. Z. The superconvergent patch recovery and *a posteriori* error estimates. Part 2: Error estimates and adaptivity. *International Journal for Numerical Methods in Engineering*, Vol. 33, pp 1365–1382, 1992.

[15] Zingg D. Grid studies for thin-layer navier-stokes computations of airfoils. *AIAA Journal*, Vol. 30, No 10, pp 2561–2564, October 1992.